JACS
JOURNAL OF THE AMERICAN CHEMICAL SOCIETY

COMMUNICATION

pubs.acs.org/JACS

Synthesis and Photocatalytic Activity of Rhodium-Doped Calcium Niobate Nanosheets for Hydrogen Production from a Water/Methanol System without Cocatalyst Loading

Yohei Okamoto,[†] Shintaro Ida,[*,†,‡] Junji Hyodo,[†] Hidehisa Hagiwara,[†] and Tatsumi Ishihara[†]

[†]Department of Applied Chemistry, Faculty of Engineering, Kyushu University, 744 Motooka, Nishi-ku, Fukuoka 819-0395, Japan,
[‡]PRESTO, Japan Science and Technology Agency (JST), 4-1-8 Honcho Kawaguchi, Saitama 332-0012

Supporting Information

ABSTRACT: Rhodium-doped calcium niobate nanosheets were synthesized by exfoliating layered $KCa_2Nb_{3-x}Rh_xO_{10-\delta}$ and exhibited high photocatalytic activity for H_2 production from a water/methanol system without cocatalyst loading. The maximum H_2 production rate of the nanosheets was 165 times larger than that of the parent Rh-doped layered oxide. The quantum efficiency at 300 nm was 65%. In this system, the methanol was oxidized to formaldehyde (main product), formic acid, and carbon dioxide by holes, whereas electrons cause the reduction of water to H_2. The conductivity of the parent layered oxide was decreased by doping, which indicates the octahedral RhO_6 unit in the lattice of the nanosheet functions as an electron trap site. The RhO_6 units in the nanosheet probably also act as reaction sites for H_2 evolution.

Hydrogen production using semiconducting photocatalysts such as NiO-loaded La-doped $NaTaO_3$ and $Rh_{2-y}Cr_yO_3$-loaded $(Ga_{1-x}Zn_x)(N_{1-x}O_x)$ has attracted attention as a clean solar hydrogen-generation system.[1,2] High crystallinity and high surface area are important properties required for high efficiency photocatalysts. A two-dimensional single crystal sheet (nanosheet) prepared by exfoliation of a layered metal oxide is an ideal material that can satisfy both of these requirements.[3−10] For instance, Pt-loaded $[Nb_6O_{17}]^{4-}$, Rh_2O_3-loaded $[Ca_2Nb_3O_{10}]^-$, and Pt-loaded $[Ca_2Nb_3O_{10}]^-$ nanosheets have been reported to exhibit high catalytic efficiency, where Pt and Rh_2O_3 act as cocatalysts.[3−10] The photocatalytic activity is strongly dependent on the cocatalyst and the loading method or process, so that a catalyst without cocatalyst or with too much cocatalyst has poor photocatalytic activity.[11,12] The role of these cocatalysts is the introduction of active sites and the promotion of charge separation. Another method to improve the catalytic activity is doping with transition metals such as Zr-doped $KTaO_3$ and Rh-doped $SrTiO_3$ systems, where the transition metal doping is performed to control the concentration of electrons and/or to improve the visible light response.[13,14] However, doping of only transition metals in catalysts without cocatalyst loading does not generally cause a significant improvement in activity compared to that with cocatalyst loading. One reason for this could be that most of the dopants in bulk such as Zr-doped $KTaO_3$ and Rh-doped $SrTiO_3$ have an indirect effect on the reaction on the surface, because almost all of the dopants are present within the catalyst, rather than on the catalyst surface. In contrast, all dopants in a nanosheet are present very close to the surface, because the thickness of the nanosheet is approximately 1 nm. Therefore, most of the dopants in a nanosheet can be expected to be directly involved in the catalytic reaction and cause a significant improvement in photocatalytic activity in the same manner as cocatalyst loading.

In this study, we report on the preparation and photocatalytic properties of Rh-doped calcium niobate nanosheets, which exhibited high activity for H_2 production from a water/methanol system without cocatalyst loading.

Figure 1 shows the crystal structure of a Rh-doped calcium niobate nanosheet prepared by exfoliating layered $KCa_2Nb_{3-x}Rh_xO_{10-\delta}$. Most of the RhO_6 units in the nanosheet can be in direct contact with the reactants. The $KCa_2Nb_{3-x}Rh_xO_{10-\delta}$ (x = 0−0.15) powder was prepared by a solution method. Next, the $KCa_2Nb_{3-x}Rh_xO_{10-\delta}$ was converted into the protonated form by acid-exchange processing using a 5 M HNO_3 solution. A colloidal calcium niobate nanosheet suspension was obtained by stirring the protonated form in a tetrabutylammonium hydroxide solution (see Supporting Information).

The color of the starting material was bright green, but the nanosheets solution was yellow. Nanosheets prepared from $KCa_2Nb_{3-x}Rh_xO_{10-\delta}$ are referred to as a Rh(x)-doped Ca−Nb−O sheet in this investigation.

The XRD patterns of the Rh-doped $KCa_2Nb_{3-x}Rh_xO_{10-\delta}$ corresponded to the pattern of $KCa_2Nb_3O_{10}$ powder reported previously, although the XRD patterns contained weak diffraction peaks assigned to an impurity phase (see Supporting Information).[15] The impurity has little noticeable effect on the preparation of nanosheets because most of the impurities can be removed by precipitation separation. The peaks ascribed to the (200) and (220) planes were shifted to smaller angles with an increasing amount of Rh as shown in Figure 2 (a = b = 0.766 nm, 0.771 nm; x = 0, 0.03 respectively). The peak shift was also confirmed in XRD patterns of nanosheet aggregate powders (see Supporting Information). These peak shifts indicate the successful doping of Rh into the $KCa_2Nb_3O_{10}$ lattice. Rhodium may occupy Nb sites (B site) in the host perovskite layer, because the ionic radius of Rh^{3+} (0.081 nm) is slightly larger than that of Nb^{5+} (0.078 nm) and the generally six-coordination of Rh^{3+} is the same as that of the B site ion.

Received: July 29, 2011
Published: October 14, 2011

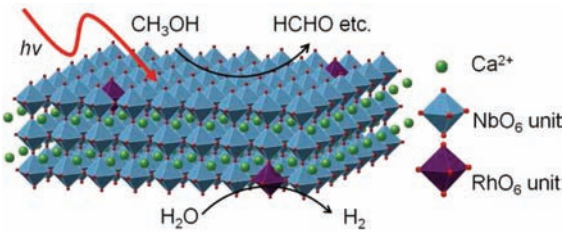

Figure 1. Crystal structure of Rh-doped calcium niobate nanosheet prepared by exfoliation of layered $KCa_2Nb_{3-x}Rh_xO_{10-\delta}$ and photocatalytic reaction model in water/methanol system.

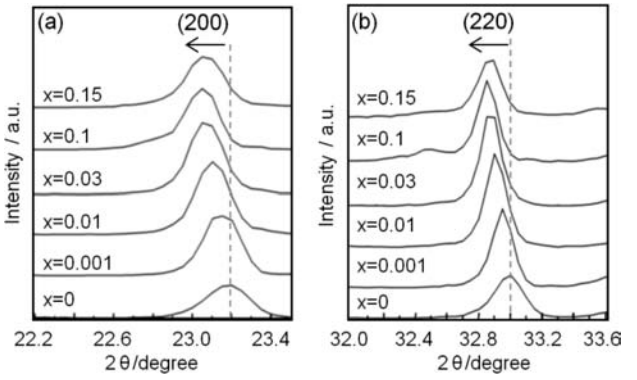

Figure 2. XRD patterns of (200) and (220) planes of $KCa_2Nb_{3-x}Rh_xO_{10-\delta}$ (x = 0, 0.001, 0.01, 0.03, 0.10, 0.15).

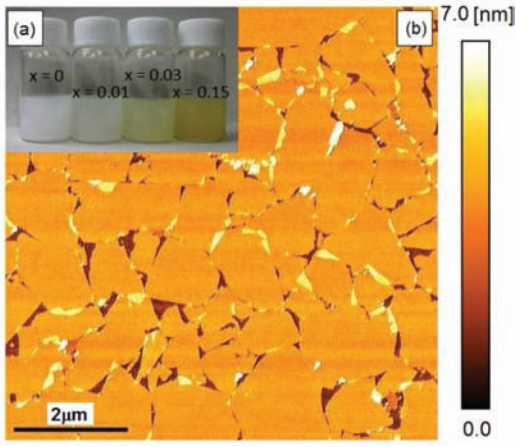

Figure 3. (a) Photograph of the Rh(x)-doped Ca−Nb−O nanosheet suspensions. (b) AFM image of monolayer film of Rh(0.03)-doped nanosheets.

Figure 3a shows photographs of the nanosheet suspensions, where the color became light yellow with increasing dopant. Exfoliation of the layered structure into individual nanosheets was confirmed by atomic force microscopy (AFM). To evaluate many nanosheets, a monolayer film of nanosheets was prepared on a Si substrate by the Langmuir−Blodgett (LB) method according to the literature.[16] A well-organized nanosheets film could be obtained when the surface pressure was 15 mN m^{-1}. Figure 3b shows an AFM image of the Rh(0.03)-doped Ca−Nb−O sheets film. The contrast of the nanosheets was homogeneous,

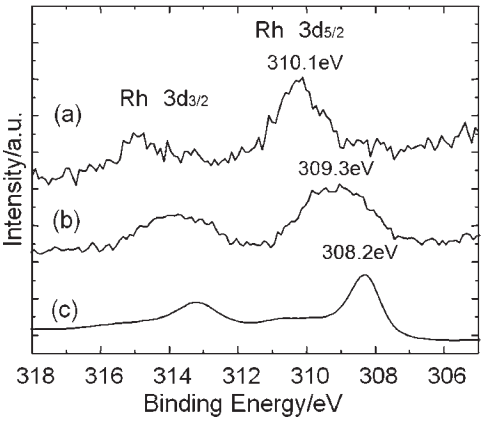

Figure 4. XPS spectra of (a) Rh(0.03)-doped Ca−Nb−O nanosheets, (b) Rh_2O_3-loaded Ca−Nb−O nanosheets, and (c) Rh_2O_3 powder.

and there were no particles on the nanosheets. The measured thickness of all the nanosheets was ∼2.8−3.0 nm, and the lateral size was ca. 1 μm. This observed thickness is about 1.5 nm larger than that of the theoretical perovskite blocks in the host solid. The thickness of the oxide nanosheets observed by AFM was generally larger than that estimated from crystallographic data,[15] because of the absorption of water and amine, and other systematic factors in the AFM measurements.

Figure 4a shows the X-ray photoelectron spectroscopy (XPS) Rh $3d_{5/2}$ narrow spectrum of the unilamella Rh(0.03)-doped Ca−Nb−O sheet. The Rh_2O_3-loaded Ca−Nb−O sheet and Rh_2O_3 are shown in Figure 4b and 4c as reference samples. The Rh_2O_3-loaded Ca−Nb−O sheet was prepared by a photodeposition method according to the literature.[4] The Rh $3d_{5/2}$ peak for Rh-doped nanosheets was at 310.1 eV, whereas the Rh_2O_3-loaded Ca−Nb−O sheet and Rh_2O_3 peaks were at 309.3 and 308.2 eV, respectively. The binding energy of Rh $3d_{5/2}$ observed in RhO_2 is at around 308.6 eV.[17] There are several interpretations to explain the shift in the binding energy position to the high energy side. One is an increase in the valence number. Another the decrease in the ratio of elements in the complex oxide, even if the valence number is the same.[18] In the case of Rh^{3+} species, the binding energy of Rh $3d_{5/2}$ is reported to be affected by the surrounding conditions, and the Rh $3d_{5/2}$ peak shifts to the higher energy side in the order of Rh_2O_3 (bulk) > Rh_2O_3 loaded on catalyst > Rh doped in the catalyst lattice.[19] Rh^{3+} $3d_{5/2}$ peaks observed in Rh-doped TiO_2 ($Ti_{0.99}Rh_{0.01}O_{2-\delta}$) and Rh_2O_3-loaded $KCa_2Nb_3O_{10}$ were at 310.0 and 309.4 eV.[4,20] The binding energy of the Rh-doped Ca−Nb−O sheet in this study is close to that of the Rh-doped TiO_2 system, which indicates that the Rh species is doped in the lattice of the nanosheet, although the valence number of Rh in the nanosheet was not determined from XPS spectra. XRD patterns indicated that the length of the *ab* axis of the lattice constant was slightly expanded by doping of Rh species, which indicates the ionic radius of Rh species is larger than that of Nb^{5+}; the ionic radius of Rh^{3+} is larger than that of Nb^{5+}, whereas ionic radii of Rh^{4+} (0.076 nm) and Rh^{5+} (0.069 nm) are smaller than that of Nb^{5+}. In light of the ionic radius of Rh and the expansion of the lattice, the valence of most Rh is likely to be +3.

Figure 5a shows a transmission electron microscopy (TEM) image and a selected area electron diffraction (SAED) pattern for the Rh(0.03)-doped nanosheet. The TEM image shows two-dimensional objects that are identified as the nanosheets. A

dx.doi.org/10.1021/ja207103j |J. Am. Chem. Soc. 2011, 133, 18034–18037

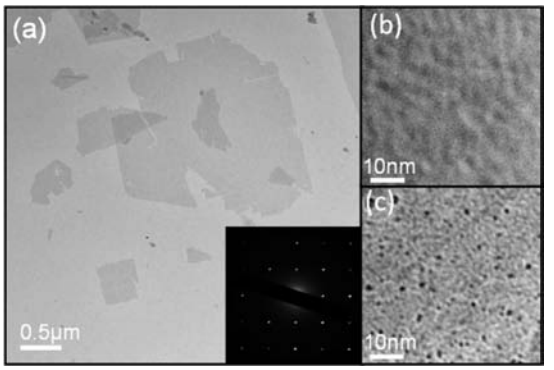

Figure 5. TEM images of nanosheets. Low magnification image and electron diffraction of Rh(0.03)-doped nanosheets (a); Rh(0.03)-doped and 0.1 wt % Rh_2O_3-loaded nanosheets at high magnification (b and c).

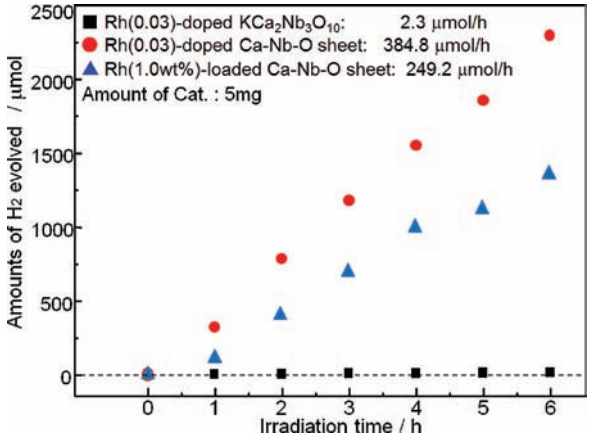

Figure 6. Time course of hydrogen evolution over (●) Rh(0.03)-doped Ca−Nb−O sheets, (■) Rh(0.03)-doped $KCa_2Nb_3O_{10}$, and (▲) Rh(1.0 wt %)-loaded Ca−Nb−O sheet. Reaction condition: 5 mg of catalyst, 150 cm^3 of aqueous 10 vol % methanol solution, 500 W Xe lamp.

square-shaped SAED pattern was observed, which indicates that the nanosheet is a single crystal. Figure 5b and 5c show magnified TEM images of the Rh(0.03)-doped Ca−Nb−O (Rh: 0.59 wt %) and Rh(1.0 wt %)-loaded nanosheets. Many fine particles of 2−5 nm in diameter were deposited on the Rh_2O_3-loaded sheets, whereas the Rh-doped sheets had no such particles. The TEM images also revealed that the Rh species are not deposited on the sheet, but are doped into the Ca−Nb−O sheet.

Figure 6 shows time courses of H_2 evolution from aqueous 10 vol % methanol solutions by photoirradiation in the presence of 5 mg of Rh(0.03)-doped Ca−Nb−O nanosheets and the parent layered oxide (Rh(0.03)-doped $KCa_2Nb_3O_{10}$). The H_2 production rate of the parent layered oxide was very low, whereas the Rh-doped Ca−Nb−O sheets exhibited high photocatalytic activity. The H_2 production rate of the nanosheets (384.8 μmol/h) was 165 times larger than that of the parent rhodium-doped layered oxide (2.3 μmol/h). However, the nondoped Ca−Nb−O sheets did not exhibit such a dramatic improvement in photocatalytic activity. The H_2 production rate with the nondoped Ca−Nb−O sheets and the parent layered oxide were 21.0 and 1.6 μmol/h, respectively (see Supporting Information). The H_2 production rate of the Rh(0.03)-doped Ca−Nb−O sheet was slightly higher (ca. 1.54 times) than that of the

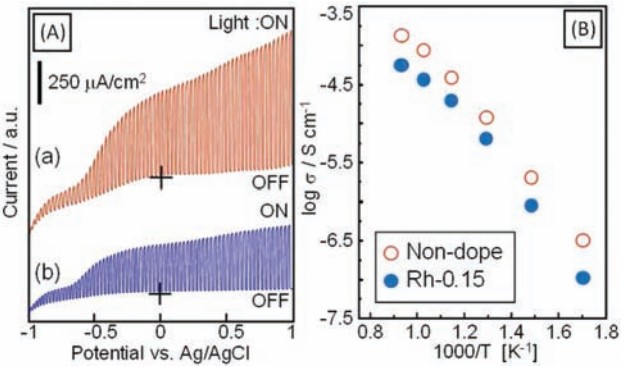

Figure 7. (A) Current−potential curves in 0.1 M Na_2SO_4 aqueous 10 vol % methanol solution under chopped light illumination (500 W Xe lamp) for (a) nondoped and (b) Rh(0.03)-doped Ca−Nb−O nanosheet/Au film. (B) Conductivity of Rh(0.15)-doped or nondoped $KCa_2Nb_3O_{10}$ as a function of temperature.

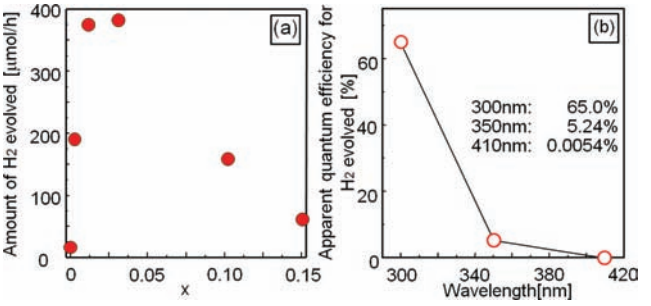

Figure 8. (a) Photocatalytic activity for H_2 production as a function of the amount of Rh(x) doping in Ca−Nb−O nanosheet. (b) Apparent quantum efficiency for H_2 generation for Rh(0.03)-doped Ca−Nb−O nanosheet.

Rh(1.0 wt %)-loaded Ca−Nb−O sheet as shown in Figure 6, which was prepared by a photodeposition method according to the literature.[4]

Figure 7A shows current−potential curves in a 0.1 M Na_2SO_4 aqueous 10 vol % methanol solution under illumination for a nanosheet/Au film, which was prepared by a layer-by-layer method according to the literature.[21] The photo-oxidation current of methanol of a nondoped sheet (Figure 7Aa) was larger than that of the Rh(0.03)-doped sheet (Figure 7Ab). This indicates that Rh in the nanosheet has little catalytic activity for the oxidation of methanol. However, photocatalytic activity of hydrogen generation increased by doping Rh in the nanosheet. This indicates that doped rhodium species act as hydrogen evolution sites. Figure 7B shows the conductivity of Rh-doped and nondoped $KCa_2Nb_3O_{10}$ as a function of temperature. The conductivity of Rh-doped $KCa_2Nb_3O_{10}$ compared to the nondoped one was lower. $KCa_2Nb_3O_{10}$ is an n-type semiconductor, and its main carrier is electrons. When Rh^{3+} ions with lower valence than Nb^{5+} are doped into $KCa_2Nb_3O_{10}$, the electrons are captured by the Rh^{3+} ions, which results in a decrease in the conductivity. Such electron concentration control by doping is considered to decrease the recombination between photoexcited electrons and holes.[13] However, most of the dopants in bulk material have an indirect effect on the reaction on the surface, because most of the dopant ions are present within the catalyst, rather than on the catalyst surface. Therefore, Rh-doped $KCa_2Nb_3O_{10}$ without cocatalysts

shows low photocatalytic activity. In contrast, most of the Rh species in the Rh-doped nanosheets are present very close to the surface because the sheet thickness is ca. 1 nm, and the RhO_6 site functions as an electron capture site. Therefore, doping Rh into the nanosheets could result in a significant improvement in photocatalytic activity.

Figure 8a shows the photocatalytic activity for H_2 production as a function of the amount of Rh doping. The Rh(0.03)-doped Ca−Nb−O sheet exhibited maximum activity. The amount of Rh in the Rh(0.03)-doped sheet corresponds to 0.59 wt % Rh in the Ca−Nb−O sheet. For the $Ca_2Nb_3O_{10}$ sheet loaded with Pt, Rh_2O_3, or NiO as cocatalysts, the optimum amount of cocatalyst is typically in the region from 0.1 to 1.0 wt %. It is interesting that the optimum amount of Rh-doping is close to that of Rh-loading. The apparent quantum efficiency for H_2 production using the Rh(0.03)-doped Ca−Nb−O sheet at 300 and 410 nm was 65 and 0.0054%, respectively, so that the apparent quantum efficiency was relatively high under UV-light illumination as shown in Figure 8b.

A model of the photocatalytic reaction mechanism in the presence of CH_3OH is illustrated in Figure 1. CH_3OH is oxidized to formaldehyde, formic acid, and carbon dioxide by photoexcited holes, whereas photoexcited electrons cause the reduction of H_2O to H_2. After reaction under illumination for 6 h, HCHO (1610 μmol), CO_2 (9 μmol), and HCOOH (1 μmol) were detected with formaldehyde as the main product due to the oxidation of methanol in the Rh(0.03)-doped nanosheet system. The HCHO was quantitated by iodometry.[22] Moreover, H_2 and D_2 evolution experimentation using CD_3OD instead of CH_3OH resulted in a H_2/D_2 mass current ratio of ~500. In the cases of the H_2O/CD_3OD system, CD_3OD was converted to CD_3OH after reaction, which is due to deuterium−hydrogen exchange between CD_3OD and H_2O. If the hydrogen evolved under illumination is due to decomposition of CD_3OD or CD_3OH, D_2 (mass 4) or HD (mass 3) should be detected. However, the main peak for the H_2O/CD_3OD system was mass 2 (H_2) (see Supporting Information). This indicates that H_2 evolution is due to the reduction of H_2O.

In conclusion, Rh-doped Ca−Nb−O nanosheets exhibited high photocatalytic activity for H_2 production from a water/methanol system without cocatalyst loading. The photocatalytic activity of the nanosheets was affected by the amount of Rh doping, and the Rh(0.03)-doped Ca−Nb−O sheet exhibited the highest H_2 production rate; the H_2 production rate was 165 times larger than that of the parent layered oxide. The apparent quantum efficiency at 300 nm was 65%. The doping of a noble metal into the nanosheet is a promising approach to improve the photocatalytic activity.

■ ASSOCIATED CONTENT

Supporting Information. XRD pattern (S1, S2), time course of hydrogen evolution data for nondoped $KCa_2Nb_3O_{10}$ system (S3), UV−vis absorption data (S4, S5), mass spectra (S6), chemical composition of the parent materials (S7), and experimental details. This material is available free of charge via the Internet at http://pubs.acs.org.

■ AUTHOR INFORMATION

Corresponding Author
s-ida@cstf.kyushu-u.ac.jp

■ ACKNOWLEDGMENT

This work was supported by the JST PRESTO program.

■ REFERENCES

(1) Kato, H.; Asakura, K.; Kudo, A. *J. Am. Chem. Soc.* **2003**, *125*, 3082–3089.
(2) Maeda, K.; Teramura, K.; Lu, D.; Takata, T.; Saito, N.; Inoue, Y.; Domen, K. *Nature* **2006**, *440*, 295.
(3) Abe, R.; Shinohara, K.; Tanaka, A.; Hara, M.; Kondo, J. N.; Domen, K. *Chem. Mater.* **1997**, *9*, 2179–2184.
(4) Hata, H.; Kobayashi, Y.; Bojan, V.; Youngblood, W. J.; Mallouk, T. E. *Nano Lett.* **2008**, *8*, 794–799.
(5) Ebina, Y.; Sasaki, T.; Harada, M.; Watanabe, M. *Chem. Mater.* **2002**, *14*, 4390–4395.
(6) Ebina, Y.; Sakai, N.; Sasaki, T. *J. Phys. Chem. B* **2005**, *109*, 17212–17216.
(7) Matsumoto, Y.; Koinuma, M.; Iwanaga, Y.; Sato, T.; Ida, S. *J. Am. Chem. Soc.* **2009**, *131*, 6644–6645.
(8) Comptons, O. C.; Mullet, C. H.; Chiang, S.; Osterloh, F. E. *J. Phys. Chem. C* **2008**, *112*, 6202–6208.
(9) Maeda, K.; Mallouk, T. E. *J. Mater. Chem.* **2009**, *19*, 4813–4818.
(10) Townsend, T. K.; Sabio, E. M.; Browning, N. D.; Osterloh, F. E. *ChemSusChem* **2011**, *4*, 185–190.
(11) Domen, K.; Naito, S.; Onishi, T.; Tamaru, K. *J. Phys. Chem.* **1982**, *86*, 3657–3661.
(12) Kudo, A.; Tanak, A.; Domen, K.; Maruya, K.; Aika, K.; Onishi, T. *J. Catal.* **1988**, *111*, 67–76.
(13) Ishihara, T.; Nishiguchi, H.; Fukamachi, K.; Takita, Y. *J. Phys. Chem. B* **1999**, *103*, 1–3.
(14) Konta, R.; Ishii, T.; Kato, H.; Kudo, A. *J. Phys. Chem. B* **2004**, *108*, 8992–8995.
(15) (a) Dion, M.; Ganne, M.; Tournoux, M. *Mater. Res. Bull.* **1981**, *16*, 1429–1935. (b) Jacobson, A. J.; Johnson, J. W.; Lewandowski, J. T. *Inorg. Chem.* **1985**, *24*, 3727–3729.
(16) Muramatsu, M.; Akatsuka, K.; Ebina, Y.; Wang, K.; Sasaki, T.; Ishida, T.; Miyake, K.; Haga, M. *Langmuir* **2005**, *21*, 6590–6595.
(17) Zhang, Y.; Grass, M. E.; Habas, S. E.; Tao, F.; Zhang, T.; Yang, P.; Somorjai, G. A. *J. Phys. Chem. C* **2007**, *111*, 12243–12253.
(18) Capitan, M. J.; Centeno, M. A.; Malet, P.; Carrizosa, I.; Odriozola, J. A. *J. Phys. Chem.* **1995**, *99*, 4655–4660.
(19) Dohmae, K.; Hirose, Y.; Kimura, M. *R&D Review of Toyota CRDL* **1997**, *32*, 75–82.
(20) Bera, P.; Hegde, M. S. *Catal. Surv. Asia* **2011**, 1–19.
(21) Izawa, K.; Yamada, T.; Unal, U.; Ida, S.; Altuntasoglu, O.; Koinuma, M.; Matsumoto, Y. *J. Phys. Chem. B* **2006**, *110*, 4645–4650.
(22) Romijin, G. *Z. Anal. Chem.* **1897**, *36*, 18–27.